A Characterization of Pulsed Electron Beam Welding Parameters

Although initially considered promising, pulsed electron beam welding proved ineffective in this experiment

BY D. D. KAUTZ, D. L. OLSON, P. BURGARDT AND G. R. EDWARDS

ABSTRACT. Interest existed in developing pulsed electron beam welding for applications in which keyhole penetration and low heat input were needed. The process parameters were checked with respect to weld penetration, conduction melting and root irregularities (*e.g.*, incomplete penetration and porosity). The results indicated that only small gains could be achieved in penetration with respect to heat input, whereas the increase in root irregularities increased greatly. It was therefore concluded that pulsed electron beam welding in a keyhole mode is not satisfactory for most welding applications.

Introduction

The use of electron beam and laser beam welding for joints where extreme precision is needed is well documented (Refs. 1, 2). On the one hand, continuous-power electron beam welding and laser beam welding are particularly well suited to applications where high weld aspect ratios are needed. On the other hand, pulsed laser beam welding is typically used for thin-section welds and designs where part heating must be minimized. The area between these regimes — welds that need deep joint penetration and minimal heat input — is not adequately addressed by either of the above processes. We studied the feasibility of using a pulsed electron beam power source to make welds of this category.

Pulsed Electron Beam Welding Parameters

Along with the standard parameters for electron beam welding, pulsed electron beam welding has its own unique parameters that must be considered: pulse frequency or period, pulse-on time, pulse amplitude and pulse shape.

The pulse frequency or period defines the rate at which beam pulses are generated. This term is mathematically continuous as the pulsed parameters approach the continuous-power limit.

The pulse-on time is the portion of the pulse period when the electron beam is emitted. The remaining pulse time (pulse-off time) is the cooling cycle for the weld metal. The smaller the ratio of pulse-on time to pulse-off time, the higher the cooling rate of the weld metal.

Since the current during pulse-off time is zero amperes, the pulse amplitude is equivalent to the current during pulse-on time. We observed some drift from zero (probably due to machine electronics) in the pulse-off time current, and we monitored it carefully during this experiment. We found no comparable drift in the pulse-on time beam current during the study.

The pulse shape generated by the welding machine was supposed to approximate a square wave. In practice, however, it rounded off as pulse frequency increased to approximate a sine wave. The rounding is shown in the oscillograms of Fig. 1, which were obtained using a Faraday cup circuit.

KEY WORDS

Electron Beam Welding
Pulsed Welding
Pulsed EBW Parameters
Low Heat Input
Root Irregularities
Spiking Phenomena
Electron Beam Pulses
Faraday Cup Circuit
Weld Penetration
Weld Keyhole Width

D. D. KAUTZ is with Lawrence Livermore National Laboratory, Livermore, Calif. D. L. OLSON, P. BURGARDT and G. R. EDWARDS are with Colorado School of Mines, Golden, Colo.

Paper presented at the 69th Annual AWS Meeting, held April 17–22, 1988, in New Orleans, La.

Previous Work

Reports on pulsed electron beam welding have focused on the solidification structures and morphology of the finished welds. Although it is known that penetration efficiency can be increased with pulsed beams, this aspect has not been thoroughly studied.

Tokmakov (Refs. 3, 4) found that large penetration increases relative to fusion-zone area can be gained with use of a pulsed beam. The penetration increase resulted from the reduction in conduction melting that occurred on the sidewalls of the weld. It developed, however, that the welding efficiency gains were also linked to increased weld spatter, which was in turn related to the formation of weld porosity.

Another study, by Slavin and Khudyshev (Ref. 5), compared the effect of cooling rates on grain refinement in the fusion zone. They found that grain size could be reduced by using pulsed welding parameters. Control of grain size in this way could be helpful for welding pure metals, in which grain growth is a severe problem. We found that this grain refinement was more than offset by the spatter and porosity problem discussed by Tokmakov.

Weld Penetration

Many equations can be used to describe heat flow during welding. Of these, probably the best to describe electron beam welding in the keyhole mode is the Rosenthal equation altered to model a Gaussian-shaped power source (Refs. 6, 7) shown as:

$$T - T_0 = \frac{Q/l}{2\pi\rho c}\int_0^\infty \frac{dt''}{2at'' + \sigma^2} \exp\left[\frac{-w^2 + y^2 + 2wvt'' + (vt'')^2}{4at'' + 2\sigma^2}\right] \quad (1)$$

where t'' = measured time increment,

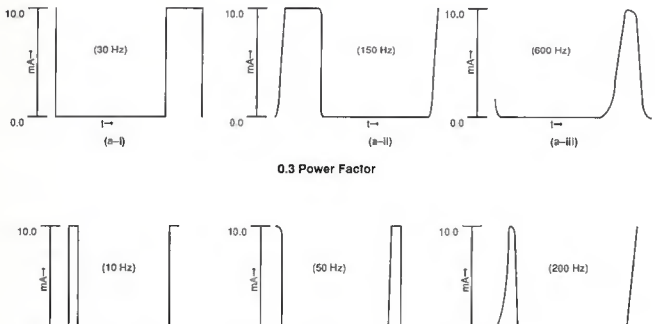

Fig. 1—Rounding of the beam-current pulse as frequency and pulse-on time change. A—Shows 0.3 power factor pulses; B—shows 0.1 power factor pulses. Pulse frequency increases from (i) to (iii) in each. The pulse-on time beam current for all welds was nominally 10 mA.

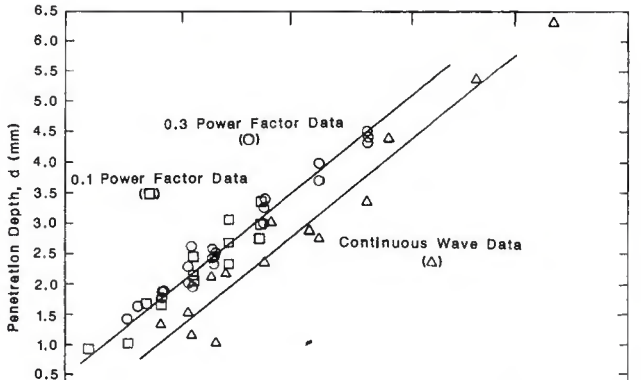

Fig. 2—Relationship showing that pulsing of the weld power increases the weld penetration with respect to total power input per length of weld section.

σ = beam distribution width, a = thermal diffusivity, v = relative workpiece velocity, Q/l = total power input per unit length, c = material heat capacity, and w = distance in the x-direction minus the heat source displacement (mm).

Equation 1 gave much better agreement with actual weld geometry data than did equations that were discontinuous at the weld centerline. The ability to use a finite beam width also enabled calculation of a finite centerline temperature for the weld. The drawback to Equation 1 is that a beam distribution width must be accurately measured. We solved this problem by using a modified Faraday cup assembly. The modified Faraday cup allows the beam to be scanned across a small mask placed on top of a conventional Faraday cup. A plot of the current flow through the mask during a scan provides a beam profile.

Equation 1 may be used to derive a relatively simple expression for weld penetration. Equation 2 applies only after steady state has been achieved. Equation 2 does, however, fit the empirical weld data in the form:

$$d = K\left[\frac{EI}{(vD)^n}\right] + c \qquad (2)$$

Table 1—Nominal Composition of Type 21-6-9 Stainless Steel

Element	Composition (wt-%)
Chromium	20.8
Nickel	7.0
Manganese	8.2
Nitrogen	0.29
Carbon	0.038
Silicon	0.49
Sulfur	0.001
Phosphorus	0.016
Oxygen	20 ppm
Iron	Balance

where d = weld penetration depth (mm), E = beam voltage (kV), I = beam current (mA), v = workpiece velocity (mm/s), D = beam diameter (mm), and K and n are related to the material thermal properties.

We hoped to be able to generate an equation similar to Equation 2 for pulsed electron beam welding parameters. The existing literature for pulsed electron beam welding has no references to equations that deal with weld geometry as a function of the welding parameters.

Experimental Procedure

Scope and Objectives

Our purposes in this study were to characterize pulsed electron beam welding and to investigate the usefulness of the process in an industrial setting. Our objective was to discover the parameter regimes in which pulsed electron beam welding would and would not produce satisfactory weldments. We planned to establish the usefulness of pulsed EB welding in an industrial environment by measuring the machine repeatability, studying the stability of the various pulsed electron beam welding parameters, and comparing the general weld quality with continuous-power electron beam welds.

Test Apparatus Setup

The test apparatus used for this experiment consisted of:

1) A high-vacuum, high-voltage Leybold-Heraeus 7.5-kW electron beam welding machine.

2) Type 21-6-9 stainless steel test plates.

3) Fixturing for parameter setup and test plate movement during welding.

4) Faraday cup and modified Faraday cup.

We set the welding parameters as suggested in the operating manual (Ref. 8) with the addition of some monitoring equipment to the normal sequence. Since the pulsing module did not work as intended, we made a slight modification in the startup sequence for the pulsed welding.

The test plates used for the welds were electroslag-refined, Type 21-6-9 stainless steel—Table 1. We chose this stainless steel for its microstructural and mechanical properties, which make it well suited to electron beam welding, and because its use would maintain continuity with other recent electron beam welding studies. Also, Type 21-6-9 stainless steel contains manganese and nitrogen, both of which are high-vapor-pressure constituents. High-vapor-pressure components may magnify void formation (Ref. 9) during an unstable welding process; this could be helpful during a parameter characterization. The test plates were 50 mm long by 6.35 mm thick (2 × 0.25 in.). These dimensions allowed steady-state welding conditions to be achieved during each weld and provided a suitable thickness range for gathering data.

The fixturing for this experiment consisted of an adjustable tungsten target, a linear drive table and a Faraday cup beam-current measurement assembly. The tungsten target was placed level with the test plate on the table. The chamber-to-work distance was held constant at 254 mm (10 in.).

We made two Faraday cup measurements before and two after each weld. The first Faraday cup measurement augmented the panel meter current value. This indicated if there were any meter calibration problems or if a poor connection had developed between the Faraday cup and the storage oscilloscope. The other measurement was a pulse-off beam current check; the beam current was zeroed and then switched on as a check of the amount of drift in the beam-generating electronics. When these preliminary measurements had been completed, we

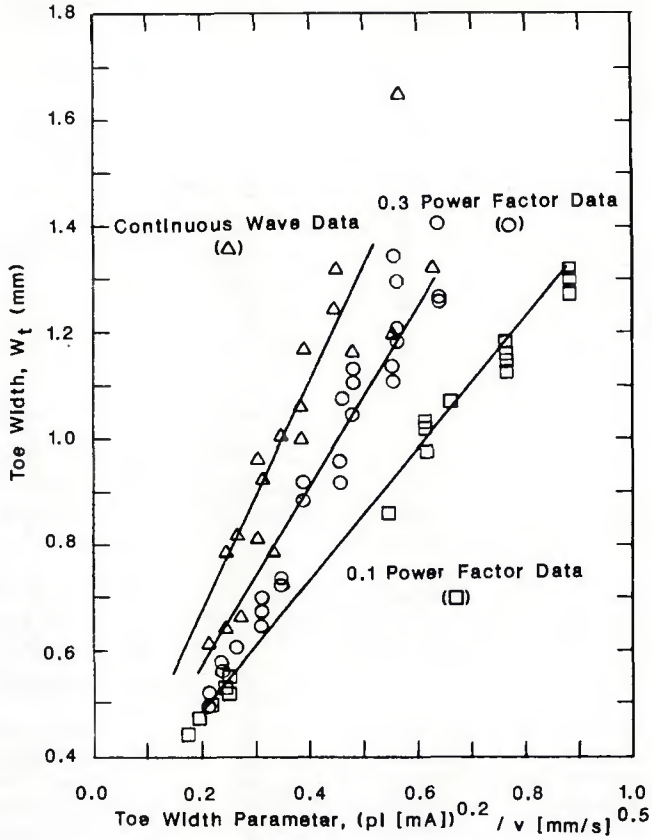

Fig. 3 — The weld data indicate that the weld toe width converges to the toe width intercept, which is believed to be related to the beam diameter. As the total power input increased, the amount of conduction heating also increased, as shown by the different slopes for each pulsing regime.

recorded the actual welding parameters on the storage oscilloscope.

We chose typical parameters used in industrial electron beam welding applications for this investigation. The travel speed, however, was greatly influenced by the use of pulsed parameters, which were comparable to pulsed laser beam welding speeds.

Results and Discussion

Penetration Depth

In electron beam welding, the measurement of interest is typically weld penetration depth. Pulsed electron beam welding was proposed as a method to decrease the total heat input to a weld area without adversely affecting the weld penetration depth. An earlier study by Tokmakov (Ref. 3) had found improvement over the expected weld penetration when pulsed parameters were used.

Figure 2 exhibits the power law expression for the weld penetration as a function of the welding parameters used in our work; three sets of welding data were compared on this graph. The data from the welds fell into two distinct groups: one for the continuous-power electron beam welds, and one for the pulsed electron beam welds. The two lines were parallel, within measurement error. No large increase in the penetration was found in the range studied.

The form of the weld penetration expression found in this experiment agrees with other work on continuous-power electron beam welding (Refs. 6, 7). When we compare pulsed welding to continuous-power welding, we must include a power factor since weld penetration is related to the average power input to the weld. We calculated two expressions for the weld data. Equation 3 relates to the continuous-power weld data:

$$d_{cp} = 3.0\frac{pI}{v^{0.6}} - 0.25 \qquad (3)$$

Equation 4 relates to the pulsed weld data:

$$d_p = 3.0\frac{pI}{N^{0.6}} + 0.5 \qquad (4)$$

where d_{cp} = continuous-wave weld penetration (mm), d_p = pulsed-wave weld penetration (mm), p = power factor, I = beam current (mA), and v = the workpiece velocity (mm/s).

Although these equations may appear similar, large differences exist. The first variable of interest is the power factor. By definition, the power factor is unity for the continuous-power equation. For pulsed welding, however, the power factor will always be less than one. We would, therefore, always expect reduced penetration when using pulsed welding parameters.

In the parameter space studied, the power factor was the only pulsing variable we found to be related to weld penetration. Pulse frequency did not affect maximum weld penetration, although it would definitely have been of consequence in considerations of average weld penetration. We did not study average weld penetration since, for normal joint specifications, it would be a meaningless value.

Workpiece velocity is another parameter that must be accounted for in a comprehensive penetration equation, and the data from our study agree well with theoretical analysis using a Gaussian-shaped power density. The exponent on the velocity seems to be material-dependent, but other work has shown that a value of 0.6 is representative for stainless steels.

Both Equations 3 and 4 have slope and intercept constants that are physically related to the experiment. The slope constant for both equations includes parameters such as beam voltage (held constant in this work) and material thermal properties. When we consider the intercepts, we must note some differences between the continuous-power and pulsed weld data.

During continuous-power operation, some power is used to heat the material from ambient conditions to the melting point. This set of conditions would support the view that the penetration intercept should be a negative value. The pulsed data, however, are related to the time needed to achieve a steady-state penetration. In the parameter space studied, the positive intercept is probably related to the large power input while the beam is on. A discontinuity in the equation will exist at some point close to the zero power level. At some point, the regime controlled by power input in our study could (and probably would) be replaced by a regime controlled by pulse-on time.

Toe Width

Another important consideration in electron beam welding is weld toe width, a practical measure of heat-conduction melting obtained with a set of welding parameters. We would expect the toe width of a pulsed weld to be smaller than that for a continuous-power weld since the weld cools between pulses. Two reasons exist for the importance of controlling the toe width: 1) the toe width is related to the nonaxial shrinkage in a finished weldment, and 2) the toe width may need controlling to maintain dimensional specifications on dissimilar thickness sections. The experimental data in Fig. 3 show that toe width did increase nominally with an increase in the average heat input.

Three expressions, Equations 5, 6 and 7, were found for the parameter space we studied. Equation 8 was related to the continuous-power weld data:

$$W_{t,cp} = 2.0\frac{(pI)^{0.2}}{v^{0.5}} + 0.24 \qquad (5)$$

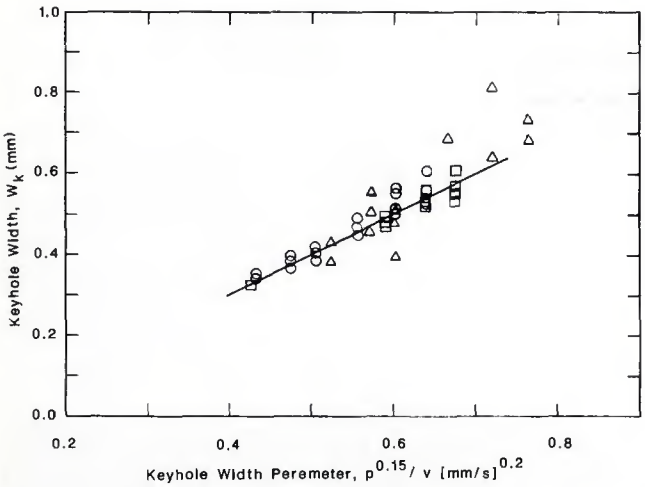

Fig. 4 — The keyhole width changed only slightly with the welding parameters. This would be expected since only a small amount of conduction heating occurred on the keyhole sidewalls. Legend: Δ — continuous-wave data, O — 0.3 power factor data, □ — 0.1 power factor data.

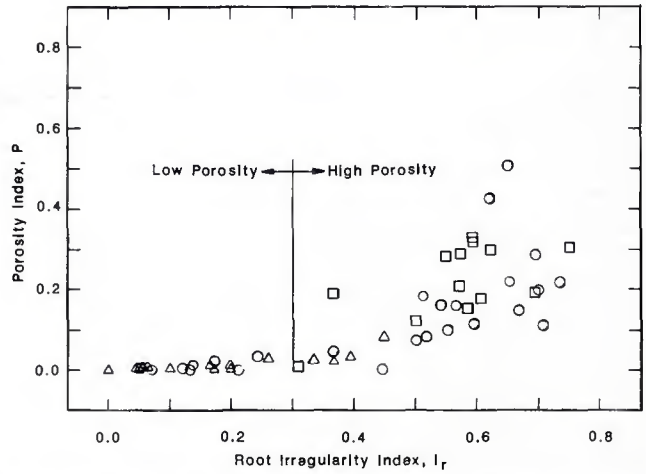

Fig. 5 — Weld data indicate two porosity regimes present in electron beam welding. Most pulsed electron beam welds had a higher root irregularity index than did the continuous-wave electron beam welds. Legend: Δ — continuous-wave data, O — 0.3 power factor data, □ — 0.1 power factor data.

Equation 6 was related to the 30% power factor pulsed electron beam welding data:

$$W_{t,30} = 1.8\frac{(pI)^{0.2}}{v^{0.5}} + 0.24 \qquad (6)$$

And Equation 7 was related to the 10% power factor pulsed electron beam welding data:

$$W_{t,10} = 1.2\frac{(pI)^{0.2}}{v^{0.5}} + 0.24 \qquad (7)$$

where $W_{t,i}$ = toe width (mm) and i = the appropriate pulsing parameter.

The intercept for the toe width is related to beam diameter rather than to welding power input, and beam diameter may be obtained from the power density profile. Other investigators (Ref. 6) have used a modified Faraday cup to measure the beam diameter at this power range to be approximately 0.3 mm. Our work agreed well with their findings.

Keyhole Width

The last fusion zone geometry consideration of interest is keyhole width. Qualitatively, we expected no appreciable change in the keyhole width from introduction of a pulsed electron beam welding source. A small width decrease could be explained by a decrease in the average power input.

Figure 4 displays the relation between electron beam welding parameters and keyhole width. As expected for a high-voltage electron beam welding process, beam current had no significant effect on keyhole width. The power factor parameter made qualitative sense in that the decrease in energy for heat conduction melting correlated with the increase in the percentage of weld pulse time apportioned to cooling.

The slower part-travel speeds allowed more heat to build up around the weld cavity, and we observed more heat-conduction melting on the keyhole sidewalls as travel speed decreased. Since all welds are made at sharp focus, the relation we found does not include the effects of beam profile. Beam power density, however, would greatly affect keyhole width. Equation 8 was calculated for all of the keyhole weld data we obtained:

$$W_k = \frac{p^{0.15}}{v^{0.2}} - 0.1 \qquad (8)$$

where W_k = weld keyhole width (mm).

Weld Discontinuities

Three categories of weld discontinuities were noted in this work: weld porosity, voids and incomplete penetration; weld root irregularities; and weld surface roughness. All of these discontinuities are considered to be detrimental to the quality of finished welds.

The voids and incomplete fusion in some welds compromised their structural integrity and ability to remain leaktight. The degradation of the material properties was related to the size and irregularity of many discontinuities (Refs. 10–12). This research found the asymmetry of the discontinuities in the welds increased with increased percentage of porosity in the welds.

In agreement with previous electron beam welding studies, we discovered that weld root irregularities were associated with the entrapment of porosity and other discontinuties (Refs. 6, 10). Figure 5 indicates that, at a root irregularity index of approximately 0.3, a threshold occurred between those welds with no or small amounts of porosity and those welds with large volumes of porosity.

Root irregularities (*e.g.*, spiking phenomena and general root oscillations) are characteristic of the melting processes involved in high-energy-density welding. Root oscillations in pulsed welding result from the constant filling of the weld cavity, caused by forces acting on the liquid metal along the back wall of the keyhole. The irregularity caused by the normal cavity-filling process is only a small percentage of the total weld depth. Although we did not observe it in this experiment, spiking can be more detrimental to overall weld quality. Spiking occurs when the normal cavity collapse does not occur during the welding cycle (Ref. 13).

Although we did not quantify the effects of surface roughness on the formation of other discontinuities, we judged qualitatively that increased surface roughness was associated with increased weld porosity. No good relation would be expected for this phenomenon since nonsteady-state conditions are involved. In our study, discontinuities such as shrinkage voids and incomplete fusion also affected the ability of pulsed welds to maintain stable penetration levels. Since porosity is more prevalent in the pulsed electron beam welds, additional studies into controlling root irregularity and weld porosity through the use of advanced electronics, *i.e.*, pulse shaping, are required before pulsed electron beam welding is used for critical welding applications.

Metallographic Results

The metallographic sections of the welds may be used to describe many of the phenomena found in pulsed electron beam welding. In general, transverse cross-sections did not offer the dimension of interest for pulsed welding. The longi-

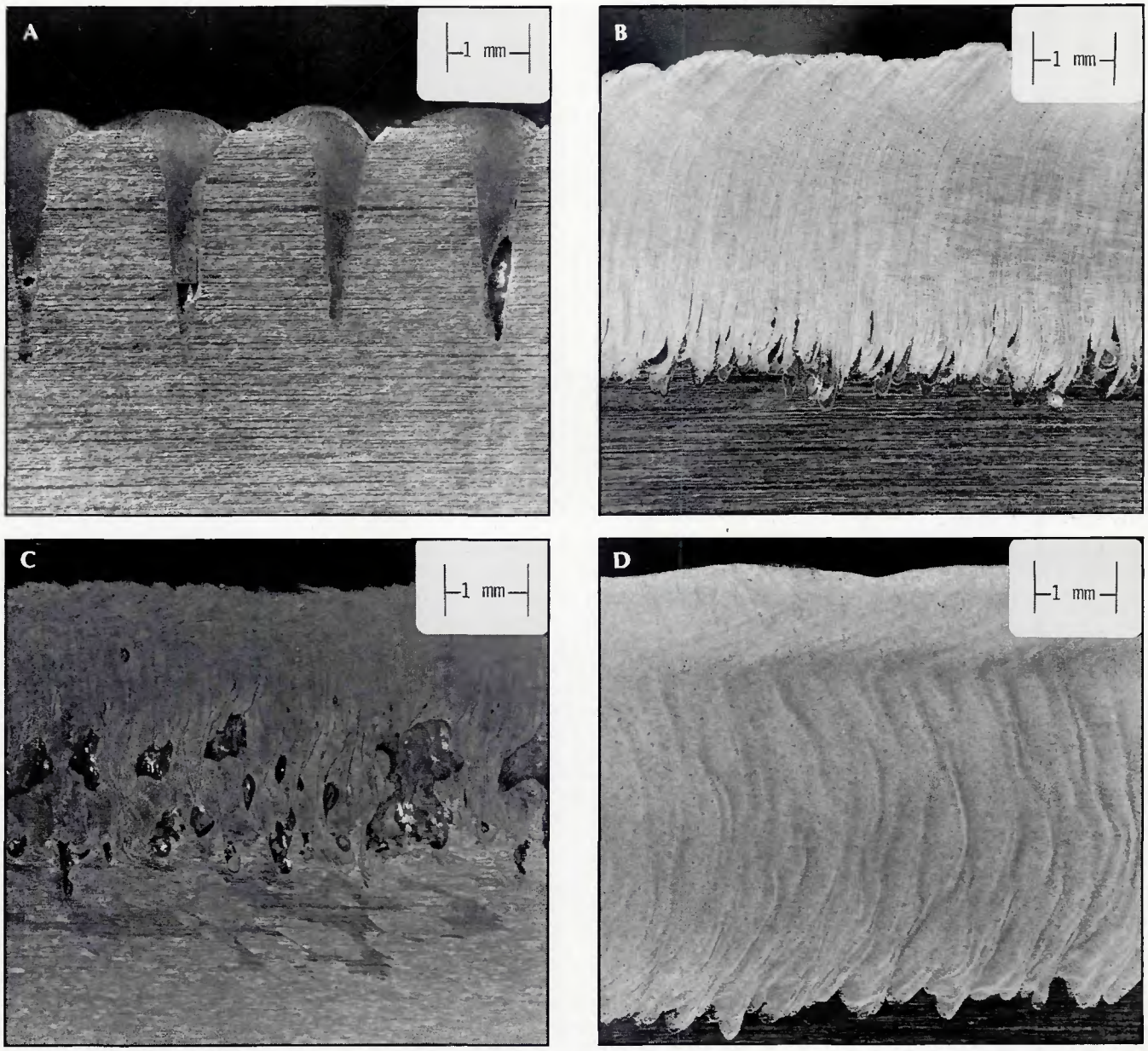

Fig. 6 — Four longitudinal metallographic sections illustrating the different regimes of electron beam welding found in this study. A — Pulsed electron beam stitched-mode weld; B — continuous-wave-like pulsed weld; C — transition-mode pulsed weld; D — continuous-wave electron beam weld.

tudinal sections, however, were excellent for comparing the weld geometry considerations that must be accounted for when using pulsed parameters. Figure 6 shows the various regimes for pulsed electron beam welding we found and compares them with a continuous-power weld.

Figure 6A illustrates a weld in which the parameters were set so that the beam pulses did not make a continuous weld. These welds also gave an indication of the steady-state melting in pulsed welds in which the spots intersected. A rather large percentage of these spot welds had porosity that could be attributed to the high solidification rates within the keyhole.

Figure 6B is a transition between the spot welds of Fig. 6A and welds in which the pulses fully tie to one another. This regime is characterized by massive amounts of weld discontinuities and penetration irregularity. Similar transitions have also been observed under some conditions when using a circular beam deflection.

Figure 6C shows the only desirable regime for using pulsed electron beam welding for deep penetration. The regime is characterized by slow travel speeds and high pulse frequencies. The weld root is relatively smooth and shows few weld discontinuities. The solidification pattern in the keyhole of this weld is of note compared to continuous-power welds — Fig. 6D. The solidification front is relatively smooth, which indicates less preheating in front of the weld keyhole. The curved shape of the continuous-power weld solidification profile indicates much larger amounts of heat buildup in front of the heat source. Without improving the electronics used in pulse generation, this looks to be the only welding regime practical in normal welding situations.

Other Concerns

We noted two other concerns about using pulsed electron beam welding. These were: 1) the calibration and measurement of the beam pulses; and 2) the drift of the beam current during use.

Measurement of electron beam pulses by use of a Faraday cup attached to a storage oscilloscope was not difficult. This instrumentation allowed the pulse shapes to be measured and documented for fu-

ture comparisons. The calibration of these pulse shapes would be extremely difficult, and the acceptable variability is not known and would not be easily determined. Since this particular welding machine offered poor control over the pulse shape, we did not study the effects of pulse-shape variability. A comparison of the pulse frequency rounding effect on some experimental Faraday cup measurements may be found in Fig. 6. As can be seen, some work needs to be done to ensure weld repeatability before these parameter types can be used industrially.

The second major concern was drift of the beam current during use. A zero current drift, caused by heating of the beam-curent-generating electronics, was very noticeable during the Faraday cup measurements. The only way we were able to alleviate the problem was to allow the machine to cool until the beam current could be switched off. This could definitely cause repeatability problems during fabrication of large quantities of parts.

Conclusions

The following conclusions were drawn from the results of this work:

1) Introducing pulsed welding parameters did not substantially affect the weld bead shape of electron beam welds.

2) The parameters for both continuous-power welding and pulsed electron beam welding are related in ways that affect the weld penetration depth, the weld toe width and the weld keyhole width.

3) The large number of weld discontinuities and poor control of the pulsing parameters are great disadvantages to using pulsed electron beam welding.

Acknowledgments

The authors wish to thank J. L. Ferreira for producing metallography and T. R. Nelson for editing the final report. The work was performed under the auspices of the U.S. Department of Energy by the Lawrence Livermore National Laboratory under contract W-7405-Eng-48.

References

1. Bakish, R., and White, S. S. 1964. *Handbook of Electron Beam Welding*. pp. 11-63, New York, N.Y., Wiley.

2. Schwartz, M. M. 1979. *Metals Joining Manual*. pp. 1-1 to 1-105, New York, N.Y., McGraw-Hill.

3. Tokmakov, V. P. 1980. The power particulars of the process of expulsion of metal during the pulsed action of an electron beam on a surface. *Automatic Welding* 33:22-24.

4. Tokmakov, V. P. 1981. The true and thermal efficiencies of pulsed electron beam welding. *Automatic Welding* 34:46-47.

5. Slavin, G. A., and Khudyshev, A. F. 1972. Certain features of the crystallization of the liquid molten pool during pulsed electron beam welding. *Automatic Welding* 25:1-11.

6. Burgardt, P., and Knaus, S. E. 1987. Private communication.

7. Fagar, T. W., and Tsai, N. S. 1983. Temperature fields produced by traveling distributed heat sources. *Welding Journal* 62(12): 346-s to 355-s.

8. *Leybold-Heraeus 7.5 kW Electron Beam Welder Operating Manual*. Enfield, Conn., Leybold-Heraeus Vacuum Systems, Inc., 1985.

9. Schauer, D. A. 1977. *Thermal and Dynamic Effects in Electron Beam Welding Cavities*. Report UCRL-52331, pp. 107-121, Livermore, Calif., Lawrence Livermore National Laboratory.

10. Arata, Y., Terai, K., and Matsuda, S. 1974. Study on characteristics of weld defect and its prevention in electron beam welding (report II). *Trans. JWRI* 3:59-78.

11. Arata, Y., Terai, K., and Matsuda, S. 1974. Study on characteristics of weld defect and its prevention in electron beam welding (report III). *Trans. JWRI*, 3:81-88.

12. Arata, Y., Terai, K., and Matsuda, S. 1975. Study on characteristics of weld defect and its prevention in electron beam welding (report IV). *Trans. JWRI* 4:85-92.

13. *The Physics of Welding*. ed. J. F. Lancaster. pp. 269-288, New York, N.Y., Pergamon, 1984.

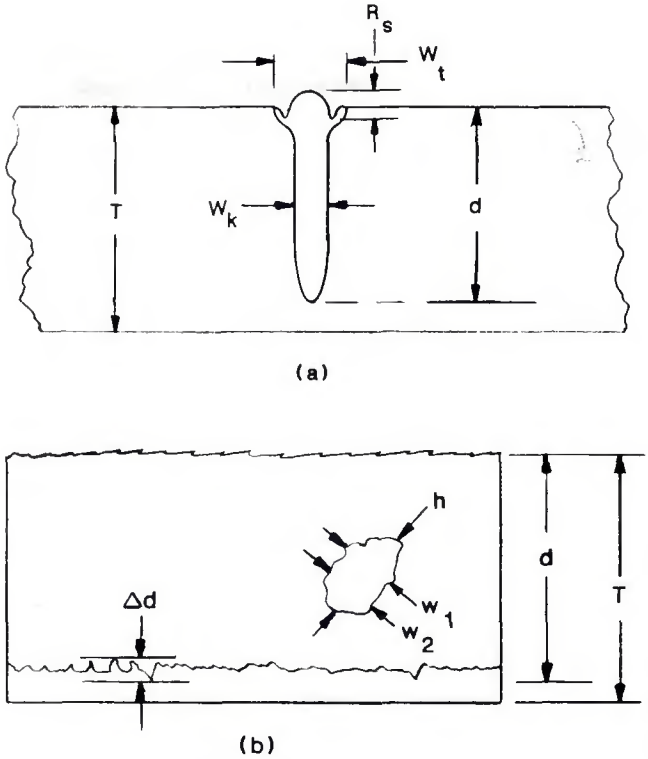

Fig. 7 — Metallographic section schematics of an electron beam weld. A — Transverse section; B — longitudinal section. Both sections have the dimensions of the experimental measurements outlined.

Appendix

The following is an alphabetical list of some of the nonstandard terms used to define the dimensions produced by pulsed electron beam welding. Terms standard to the welding industry are not included, unless the common definition has been altered to fit the welding process studied. To illustrate the terms, Fig. 7 shows two schematics that use transverse and longitudinal weld sections.

Keyhole width (W_k): The width of the fusion zone measured at the midpoint of the distance between the weld root and the weld bay.

Penetration depth (d): The maximum distance measured between the surface of the base metal and the weld root.

Power factor (p): average power ratio between a pulsed and a continuous-power weld using the same nominal parameters. The power factor for a continuous-power weld is always one. A general form for this is shown in Equation 9:

$$p = \frac{1}{\tau}\int_0^{\tau}\frac{I(t)dt}{I_{cp}} \qquad (9)$$

where τ = wave period (s), I(t) = beam current in a pulsed weld as a function of time (mA/s), and I_{cp} = continuous-power or maximum pulsed-beam current (mA).

Root irregularity index (I_r): The difference in weld penetration (Δd) along a longitudinal section, divided by the maximum penetration (d) as shown by Equation 10:

$$I_r = \frac{\Delta d}{d} \qquad (10)$$

Toe width (W_t): The distance between the weld toes.

Weld porosity index (P): The ratio of the porosity area to the weld area in a longitudinal section. For an irregular void, the approximate porosity area is calculated using Equation 11.

$$P = 0.5\,\frac{(w_1 + w_2)h}{\text{Weld area}} \qquad (11)$$

where w_i = normal void width (mm) and h = nominal void height (mm).